Scientific Research Publishing

Journal of Environmental Protection, 2023, 14, 419-440
https://www.scirp.org/journal/jep
ISSN Online: 2152-2219
ISSN Print: 2152-2197

Changes in Aerosol Optical Depth over the Arctic Ocean as Seen by CALIOP, MAIAC, and MODIS C6.1

Nicole Mölders[1,2], Mariel Friberg[3,4]

[1]Department of Atmospheric Sciences, College of Natural Science and Mathematics, University of Alaska Fairbanks, Fairbanks, USA
[2]Geophysical Institute, University of Alaska Fairbanks, Fairbanks, USA
[3]National Aeronautics and Space Administration, Goddard Space Flight Center, Greenbelt, USA
[4]Earth System Science Interdisciplinary Center, University of Maryland, College Park, USA
Email: cmoelders@alaska.edu

How to cite this paper: Mölders, N. and Friberg, M. (2023) Changes in Aerosol Optical Depth over the Arctic Ocean as Seen by CALIOP, MAIAC, and MODIS C6.1. *Journal of Environmental Protection*, **14**, 419-440.
https://doi.org/10.4236/jep.2023.146025

Received: April 27, 2023
Accepted: June 13, 2023
Published: June 16, 2023

Abstract

Due to the recent increase in Arctic shipping, 2006-2020 June to October Cloud-Aerosol Lidar with Orthogonal Polarization (CALIOP), Moderate Resolution Imaging Spectroradiometer (MODIS) Collection 6.1 (C6.1), and Multi-Angle Implementation of Atmospheric Correction (MAIAC) retrieved aerosol optical depth (AOD) data were examined for changes in AOD from period 1 (P1, 2006-2012) to period 2 (P2, 2014-2020 (P2). Herein, AOD was statistically analyzed on a 0.25˚ × 0.25˚ grid and in the airsheds over the various ocean basins over the Arctic north of 59.75˚N. According to heatmaps of the correlation between AOD and ship traffic, and AOD and fire emissions for the airsheds, all three AOD products captured the observed inter-annual variability in wildfire occurrence well, and showed wildfire emissions over Siberia were more severe in P2 than P1. Except for the Atlantic, North, and Baltic Seas, Beaufort Sea, and Barents Sea, all three AOD products indicated that AOD was higher over the various basins in P2 than P1, but disagreed on the magnitude. This fact suggests that the detection of changes in the typical low AOD over the Arctic Ocean might be rather qualitative than quantitative. While all products captured increases in AOD due to ships at berth, only MODIS C6.1 caught the elevated AOD due to shipping on the Siberian rivers. Obviously, sub-daily resolutions are required to capture increased AOD due to short-term events like a traveling ship or short-interval fire.

Keywords

Arctic Aerosol Optical Depth, Changes in Aerosol Optical Depth, Arctic Ship-Emissions Impacts on AOD, Boreal Wildfire Impacts on AOD

1. Introduction

In the maritime Arctic, aerosols stem from both natural and anthropogenic emissions. In winter and early spring, the so-called Arctic Haze includes an advection of pollutants and aerosols emitted in mid-latitudes [1] [2]. In summer, natural Arctic aerosol contains more than 50% oceanic sea-salt mass fraction, 30% - 35% mineral dust, and lower fractions of non-sea-salt sulfate, methane sulfonic acid, and biomass burning products. In summer and early fall, Arctic shipping releases primary aerosols and aerosol precursor gases like sulfur dioxide (SO_2), nitrogen oxides (NO_x = NO + NO_2 nitrogen monoxide, nitrogen dioxide), and volatile organic compounds (VOC) into the marine and coastal atmospheric boundary layer (ABL) [3] [4] [5]. Here secondary pollutants and/or secondary aerosols form through chemical reactions, gas-to-particle conversion and accumulation [6]. In addition, year-round anthropogenic emissions occur in the Arctic due to offshore oil/gas activities (e.g. flaring, traffic to or from oil platforms) [7] [8], and Arctic communities [9].

The long record of, on average, decreasing sea-ice extent [16] [17] (**Figure 1(a)**) has provided shortcuts for intercontinental transportation [18]. Therefore, over the last decade, Arctic ship traffic has notably increased (**Figure 1(b)**). Last-chance tourism, shipping of supply for support of offshore oil- or gas-related activities and Coast Guards traffic have increased as well [19] [20] [21] [22] [23]. Analysis of the 1990 to 2012 ship-activity data in the Vessel Traffic Reporting Arctic Canada Traffic Zone (known as the NORDREG zone), for instance, revealed monthly increases in ship traffic of up to 22 vessels per decade in July, and eight vessels per decade annually for government vessels, icebreakers and pleasure crafts [17]. Data collected in the Bering Strait indicated increased traffic from cargo vessels, tugs, tankers and bulk ships [24]. **Figure 1(d)** exemplarily shows the annual ship density for 2020 with the ship positions on May 9, 2023, superimposed.

Observations at Ny-Ålesund, Norway, revealed the effects of ship emissions on summertime aerosols [25] [26]. Air-quality model simulations assuming just biogenic and cruise-ship emissions affirmed that even two days after the visit of a 1000-passenger cruise ship in Glacier Bay, Alaska, concentrations of fine and coarse particulate matter ($PM_{2.5}$ and PM_{10}) and precursor gases like SO_2 and NO_X were still 77%, 85%, 85%, and 82% higher than the natural background in the ABL [27] leading to a 46% higher haze index despite the use of low-sulfur fuel [28].

In Arctic waters, however, the lack of regulations for ship emissions permits shipping companies to use (cheap) low-quality, high-sulfur bunker oils that cause high emissions, especially of soot [27] [29]. Maneuvering, and sailing at low-engine load yield incomplete combustion and high soot emissions, especially with low-quality fuel [27] [29] [30]. Anthropogenic soot aerosols, however, appreciably enhance aerosol optical depth (AOD) and yield high Ångström exponents; increases in aerosol amount and size can have substantial impacts on

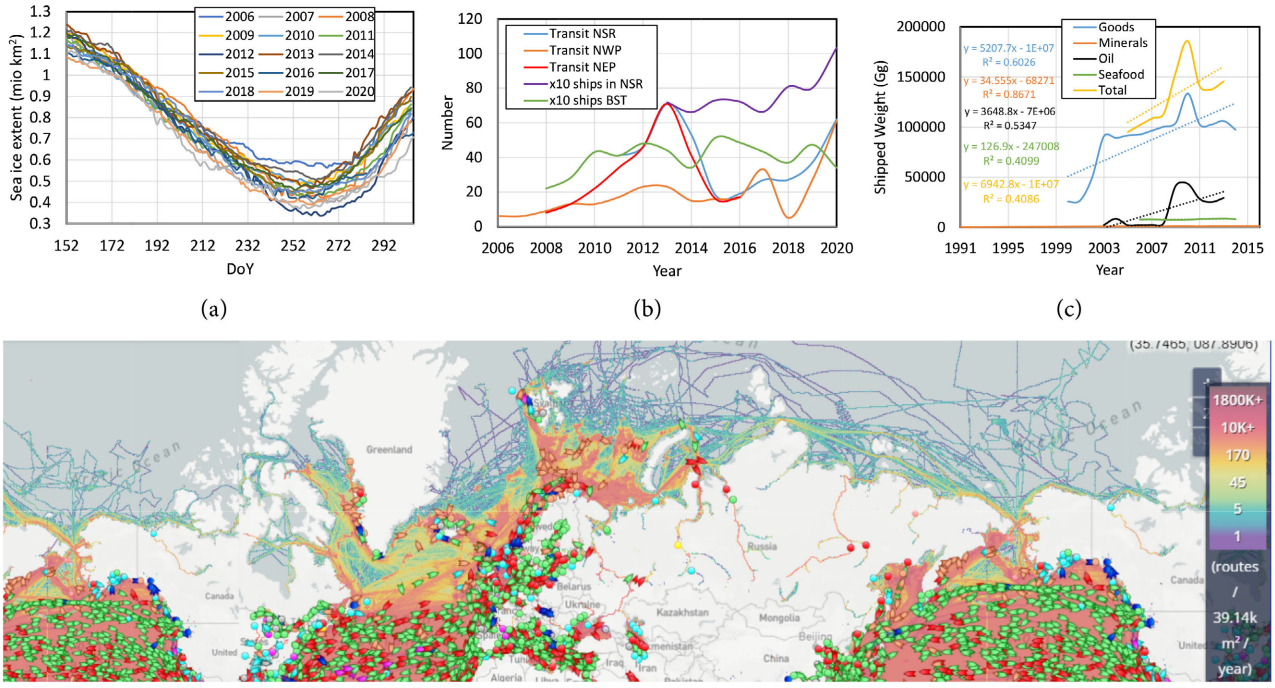

Figure 1. (a) Multisensor Analyzed Sea Ice Extent (MASIE) for June 1 to October 31 (JJASO) 2006-2020, (b) Northern Sea Route (NSR), Northwest Passage (NWP), Northeast Passage (NEP), Bering Strait transits/number of ships, (c) 1991-2016 shipped weight, and (d) collage of annual density of ships in 2020 (color shades) and snapshot of ship positions on May 9, 2023. Green, red, pink, orange, yellow, blue, and cyan are cargo vessels, tanker, pleasure crafts, fishing vessels, high speed crafts, passenger vessels, and tugs/special crafts. Data from [10]-[15].

visibility, cloud and precipitation formation as well as radiation with consequences for the local climate of the region (cf. e.g. [1] [6] [27] [31] [32] [33] [34]). Air-quality simulations, for instance, showed that an increase of the quota for cruise-ship entries in Glacier Bay by 35% (from 184 to 248 entries) would increase the haze index and reduce visibility by 7% [28].

In contrast to mid-latitudes, atmospheric conditions in high latitudes diverge significantly. Above 60˚N, atmospheric stratification is highly stable year-round and surface inversions occur more frequently. These conditions suppress mixing and reduce dry deposition and sedimentation [35]. Inversion layers over ice and/or cold water are often decoupled from the free atmosphere leading to different chemical compositions close to the surface and aloft [36] [37]. North of the Arctic Circle, the solar radiation that initiates the photochemistry [6] exists for extended periods and is as high as 24 hours around the summer solstice. The longer daylight hours also mean more time for direct aerosol effects on solar radiation (scattering, absorption), impacting the regional radiation budget [37].

North of 60˚N, surface aerosol concentrations were observed at only 40 sites for several years, but at different times since 1972 [37]. Of these, only 12 are less than 100 km from the ocean. At Utqiaġvik (formerly Barrow), Alert, Ny-Ålesund, Hornsund, and Andenes (all close to the ocean), the 1977-2006 summer background AODs at 500 nm were below 0.15 except during episodes of wildfire

smoke [38]. These background values serve as a baseline for the Arctic coastal regions. Over water only a few aerosol measurements exist from research cruises (e.g. [35] [39]). The recent and anticipated increase in Arctic shipping [40] provides a need for monitoring and predicting changes in Arctic atmospheric composition because aerosols play a role as climate forcers due to direct and indirect impacts on radiation [35] as well as impacts on cloud and precipitation formation [34].

Given the increase in Arctic shipping and oil-related/gas-related activities (**Figure 1(a)**), we hypothesized that increased ship emissions changed the atmospheric composition in areas of traffic hotspots like the Bering Strait, and new oil/gas activities. Because ground-based AOD observations are sparse in the Arctic, we tested our hypothesis using three different AOD products derived from satellite-borne instruments. Therefore, we examined June to October (JJASO) Cloud-Aerosol Lidar and Infrared Pathfinder Satellite Observations (CALIPSO) version 4 Level 2 [41] [42] [43], Moderate Resolution Imaging Spectroradiometer (MODIS) Collection 6.1 (C6.1) [44], and Multi-Angle Implementation of Atmospheric Correction (MAIAC) Level 2 [45] [46] data for changes in AOD over the Arctic Ocean between 2006-2012 and 2014-2020 shipping seasons. Typically, the Arctic shipping season starts as early as June and ends in late October.

2. Experimental Design

MODIS is onboard of Aqua and Terra, while the Cloud-Aerosol Lidar with Orthogonal Polarization (CALIOP) is on CALIPSO. Aqua and CALIPSO have been part of the A-train constellation since May 2002 and April 2006, respectively, and are on a sun-synchronous orbit ascending the equator South-to-North at ~13:30 local time. Since December 1999, Terra has been in a sun-synchronous orbit descending from North-to-South over the equator at ~10:30 local time. The orbits repeat the same ground track (±10 km) every 16 days. In some Arctic regions, overpasses overlap.

2.1. Data of AOD Products

MODIS onboard of both Terra and Aqua has collected data in 36 spectral bands ranging from 40 to 1440 nm. We use cross-calibrated Terra and Aqua MODIS C6.1 and MAIAC data and consider the MODIS instruments of Terra and Aqua jointly as a single sensor. Both the MAIAC and MODIS C6.1 products provide AOD at 550 nm.

We used the MODIS C6.1 Level 2 aerosol products (MOD04 for Terra and MYD04 for Aqua) at a 3 km resolution [47].

The MAIAC retrieval uses MODIS data for time-series analysis and a combination of pixel-based and image-based processing to improve the accuracy of cloud detection, aerosol retrievals and atmospheric correction for surface retrievals. The MAIAC products are on a fixed sinusoidal projection grid at a 1-km

increment. They include, among others, AOD, aerosol type (background, biomass burning, dust), and Ångström parameter. See [45] [46] for more information on the MAIAC retrieval algorithm.

CALIOP is a dual wavelength (532 nm, 1064 nm), polarization-sensitive backscatter lidar. It provides, among others, information on vertical aerosol distributions along CALIPSO's paths. We used the column-integrated tropospheric and stratospheric optical depths. For details of the retrieval algorithm see [48].

Within the framework of an investigation on the impact of temporal and spatial scales of AOD products over the Arctic (north of 59.75˚N), the June 1 to October 31 (JJASO) 2006-2020 MODIS C6.1, MAIAC, and CALIOP retrieved AOD values were evaluated using collocated aerosol robotic network (AERONET) AOD-data from 35 sites [49]. The major findings were as follows. MAIAC showed the best performance over land followed by MODIS C6.1. MAIAC had the highest amount of missing data over the ocean. The MODIS C6.1 product typically provided higher AOD values than the other two products. Furthermore, 70.8%, 59.5% and 64.5% of the CALIOP, MAIAC, and MODIS C6.1 retrieved AOD values fell within the expected error (EE) of the AERONET-derived AOD values. The MODIS C6.1 product showed the most details in spatial and temporal AOD distribution. Typically, the correlation between CALIOP and AERONET AOD was weak for AOD at 532 nm (less than 0.05), and increased with increasing JJASO 2006-2020 mean AOD. Considering all sites and years, the JJASO MAIAC- and AERONET retrieved AOD at 550 nm correlated moderately ($R \geq 0.4$). A strong ($R \geq 0.6$), and very strong ($R \geq 0.8$) was found at three sites for both products. AERONET and MODIS AOD values showed very strong and strong correlations at seven and four sites, with moderate correlations over all sites and JJASO 2006-2020 [49]. There were no significant differences between AERONET and the spaceborne AOD products for 2006-2012, 2014-2020 and 2006-2020. Consequently, we can examine changes in atmospheric composition in relative terms.

An evaluation by measurements from the marine aerosol network (MAN) and 15 coastal AERONET sites north of 59.75˚N revealed that 75.3% of the JJASO 2006-2018 MODIS C6.1 AOD values fell within the EE.

To further assess AOD changes due to the potential impacts of sea-ice extent and wildfire emissions on AOD over the Arctic, we used data from the Multi-sensor Analyzed Sea Ice Extent (MASIE) [50] at 4×4 km^2 increment and Global Fire Emission Directory Version 4.1 [51].

2.2. Data Processing

To assess the changes in AOD at 550 nm, we converted the CALIOP AOD to this wavelength by applying the same procedure described in [52]. Then, we resampled the CALIOP, MODIS C6.1, and MAIAC AOD data onto the same fixed $0.25^\circ \times 0.25^\circ$ grid using a Drop-in-Bucket method.

To examine whether AOD products can detect impacts from ship traffic in AOD we calculated the JJASO means, means, medians and higher moments for each grid cell and year. Then, we examined these spatial distributions as follows.

If ships cruised in the area, the means and standard deviation should be elevated as compared to the Arctic-wide value or background value, the right-hand tail of the AOD distribution should show outliers, and the difference between minimum and maximum AOD should be large as well.

To further assess changes in atmospheric composition, we divided all gridded datasets into two periods, P1 (2006-2012), and P2 (2014-2020). In the analysis, P1 served as the baseline to which we compared P2. Monthly and JJASO averaging were applied to P1 and P2 to enhance the signal-to-noise ratio [53]. The moments of P1 and P2 were compared at the various temporal (monthly, JJASO, period) scales to gain insights into: 1) the AOD changes; 2) the impact of averaging on the detection of the changes across the products.

To further examine the reliability of the determined ship-emissions impacts on AOD, the period median AOD at each grid cell was subtracted from the grid cell's period mean AOD. After removing all negative values, the remaining values were examined to determine whether they featured a distribution similar to the typical shipping routes, and/or showed the traffic hot spots (see e.g. **Figure 1(d)** for frequently used routes). We also examined whether we could detect the signals from ship emissions at shorter time scales than the period resolution (e.g., period-monthly scale, JJASO inter-annual scale). A two-tail Student's t-test was performed to examine the various P1 and P2 datasets at the different temporal scales for significant changes at various confidence levels (90%, 95%, 99%).

Furthermore, we determined the AOD in the airsheds over the ocean basins shown in **Figure 2** for each AOD product. Then heatmaps were created to

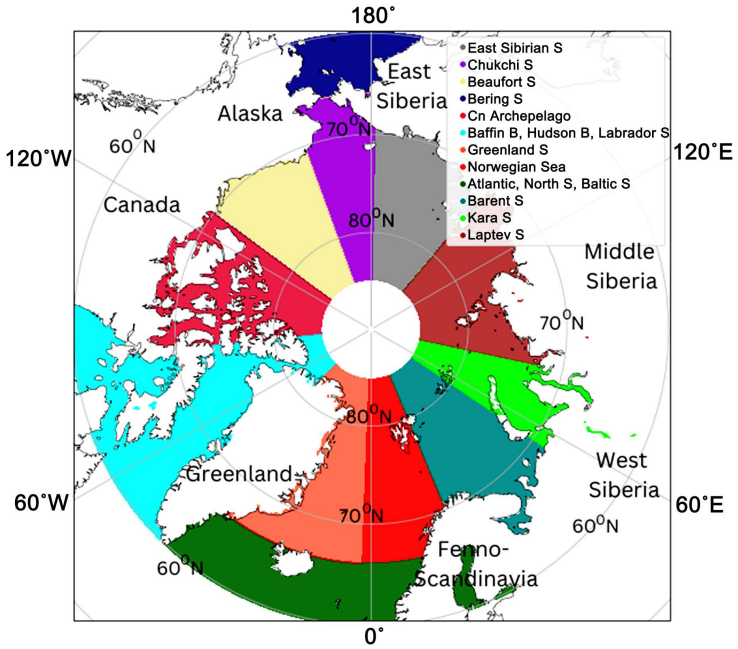

Figure 2. Map of airsheds considered in the analysis of AOD over the Arctic Ocean. The letters Cn, S and B stand for Canadian, Sea and Bay. Along a longitude, 1˚ is 110.574 km in S-N-direction, while along a latitude 1˚ in W-E-direction corresponds to 55.66 km, ~38.074 km and 19.331 km at 60˚N, 70˚N, and 80˚N.

examine the correlation between the AOD airsheds and 1) ship counts within a given sea route, 2) transit counts, 3) area burned in Alaska, Canada, Fenno-Scandinavia, and regions in Siberia, 4) mean sea-ice extent, and 5) minimum sea-ice extent. The heatmaps also served to examine JJASO-AOD anomalies in the airsheds during P2 with respect to P1.

3. Results and Discussion

The resampled mean JJASO AOD values showed that on average, MODIS C6.1 AOD exceeded that of MAIAC in most airsheds, and CALIOP had the lowest values (Table 1).

Elevated AOD values generally occurred over and downwind of the Siberian, Canadian, and Alaskan wildfires for all three products (cf. e.g. Figure 3). Typically, MAIAC provided higher JJASO means over wildfires than MODIS C6.1, but the area with high AOD values was smaller. In 2006, MODIS C6.1 and MAIAC displayed elevated AOD over the North Slope (up to 0.3). Over the Kara and Laptev Seas, JJASO means reached up to 3 for both retrievals, whereas CALIOP yielded means up to about 0.4. In the Kara Sea and Laptev Sea airsheds,

Table 1. JJASO 2006-2020 mean, and standard deviation (StDev) of AOD for various airsheds over the Arctic Ocean and Arctic-wide (land and ocean) as obtained from CALIOP, MAIAC, and MODIS C6.1.

Airshed	Aerosol optical depth					
	CALIOP		MAIAC		MODIS C6.1	
	Mean	StDev	Mean	StDev	Mean	StDev
West Arctic Ocean	0.049	0.091	0.097	0.045	0.111	0.115
East Arctic Ocean	0.045	0.078	0.089	0.059	0.132	0.175
East Siberian Sea	0.029	0.048	0.090	0.071	0.175	0.284
Chukchi Sea	0.032	0.053	0.088	0.067	0.150	0.238
Beaufort Sea	0.029	0.053	0.070	0.056	0.163	0.332
Bering Sea	0.063	0.138	0.091	0.042	0.121	0.061
Canadian Archipelago	0.033	0.052	0.090	0.066	0.135	0.221
Baffin & Hudson Bays, Labrador Sea	0.051	0.095	0.096	0.043	0.098	0.042
Greenland Sea	0.031	0.055	0.071	0.046	0.093	0.078
Norwegian Sea	0.037	0.060	0.075	0.051	0.095	0.087
Atlantic, North & Baltic Seas	0.062	0.094	0.109	0.037	0.108	0.032
Barents Sea	0.034	0.055	0.068	0.037	0.100	0.085
Kara Sea	0.033	0.057	0.070	0.056	0.134	0.211
Laptev Sea	0.029	0.045	0.088	0.087	0.176	0.321
Entire Arctic	0.038	0.090	0.087	0.101	0.164	0.153

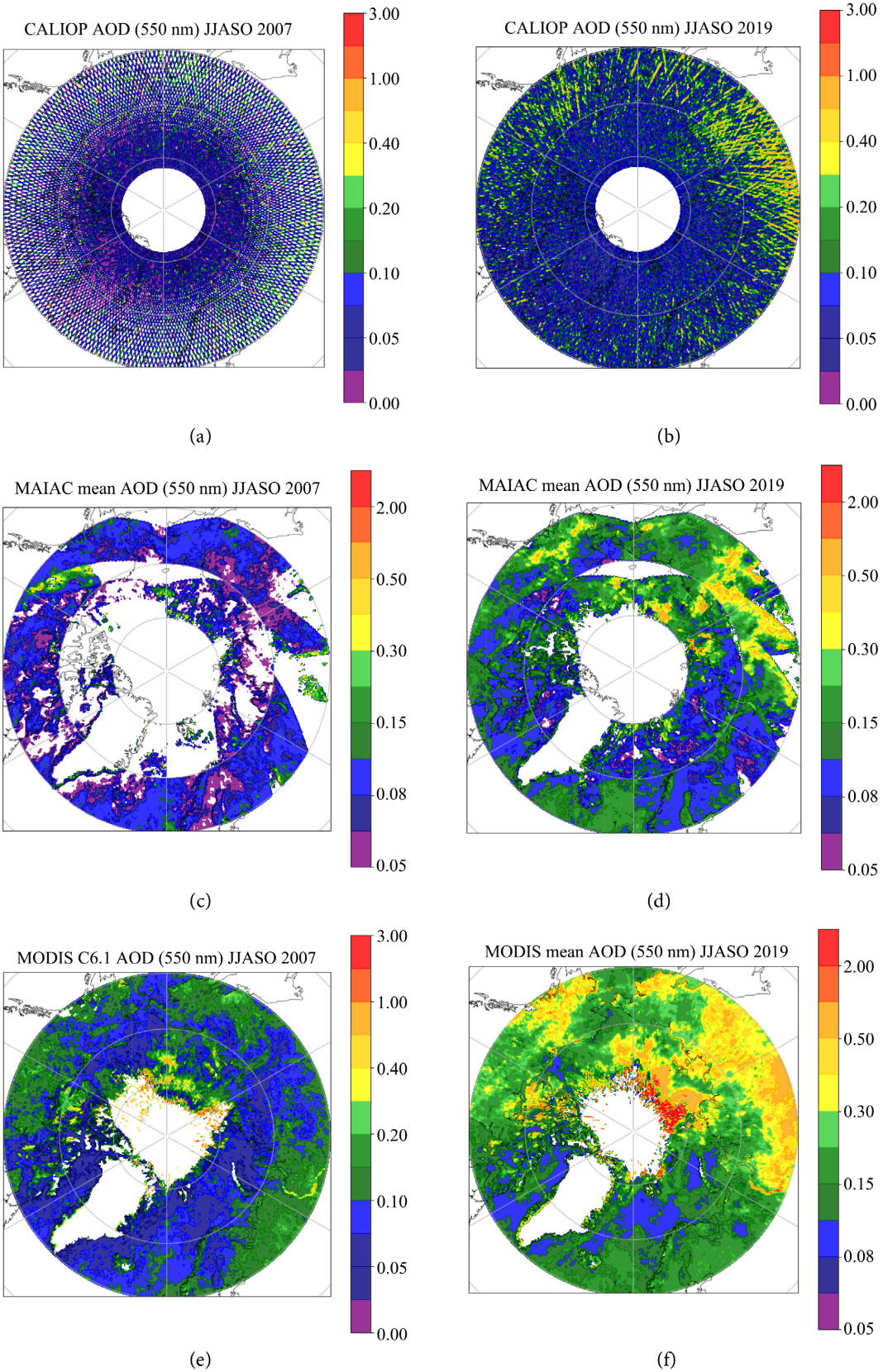

Figure 3. Comparison of JJASO mean spatial distribution of AOD (a), (c), (e) in the low fire year 2007 and (b), (d), (f) strong fire year 2019 for (a), (b) CALIOP, (c), (d) MAIAC, (e), (f) MODIS C6.1.

MODIS C6.1 JJASO-AOD means exceeded those retrieved over the West Siberian wildfires. This increase can be explained by gas-to-particle conversion during transport. CALIOP JJASO means over western Siberia reached up to 2 locally.

The substantial amounts of aerosols transported poleward and over the Pole were captured by MODIS C6.1 and less so by CALIOP or MAIAC products (Figure 3). The reasons for the detection differences are as follows. Because CALIOP collects data along the nadir, it cannot reach the farther northward air columns like the MODIS cross-track scanning instrument. The MAIAC-retrievals had fewer data, especially over the Arctic Ocean sea-ice, as the product excludes data collected at low Sun angle and over highly reflective surfaces.

2007 and 2019 were the years with the lowest and highest area burned (Figure 4). MODIS C6.1 JJASO AOD means of 2007 were elevated over the Ob, the East Siberian Sea, and in the southwest of the seaport of the Red Dog Mine in the Chukchi Sea and the Bering Sea. MAIAC JJASO means of AOD reached up to 0.4 around Svalbard, over the Canadian Archipelago, Severna Zemlya, and New Siberian Islands as well as along the ice edge. Along the coasts, AOD was less than 0.125.

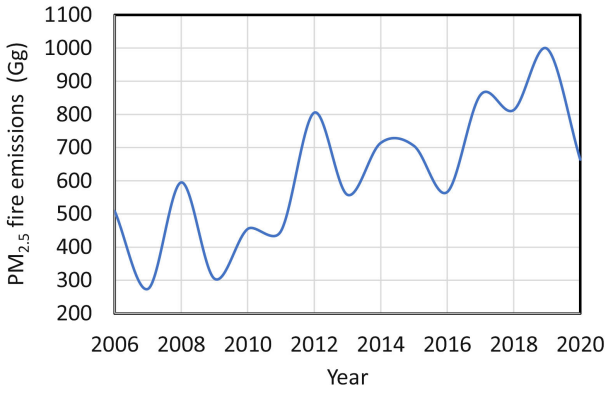

(a)

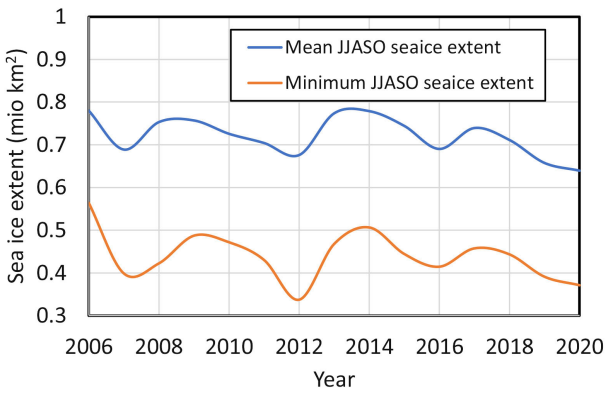

(b)

Figure 4. Timeseries of (a) wildfire emissions of $PM_{2.5}$ [51], and (b) JJASO mean and minimum Arctic sea-ice extent according to the MASIE 4 × 4 km² data [50].

In 2019, the heavy ship traffic on the Siberian rivers and traffic from the Red Dog Mine's seaport to Asia remained detectable by MODIS C6.1 despite strong fire emissions. The AOD ship emissions signals were undetectable in the MAIAC and CALIOP products in 2007 and 2019 (**Figure 3**).

3.1. AOD Sensitivity to Wildfires

Overall 15 years, 2007 had the least wildfire emissions, while 2016 had the least (**Figure 4(a)**). In Siberia, 2006, 2011, 2013, 2014, 2016, 2017, 2018, and 2019 were strong fire years. In Canada, strong fires occurred in 2014, 2015, 2016, 2017 and 2019. Alaska experienced strong fire seasons in 2010 and 2015 (cf. e.g. [51]).

In general, correlations between the area burned and airshed AOD were lower for the CALIOP product than the other AOD products (**Figure 5(a)** and **Figure 5(c)** and **Figure 5(e)**). A moderate correlation existed for the CALIOP retrieved AOD of the entire Arctic with the burned area in Siberia, especially in East Siberia and the East Arctic (**Figure 5(a)**). AOD in the airsheds over the Eastern Arctic Ocean, Atlantic, Baltic, North and Laptev Seas correlated moderately with the area burned in Fenno-Scandinavia. While the MAIAC product confirmed the latter finding (**Figure 5(c)**), it suggested a slightly lower relation between Fenno-Scandinavian area burned and the AOD over the adjacent airsheds than the CALIOP product. However, according to the MAIAC- and MODIS C6.1 products a strong correlation existed between the AOD over the Labrador Sea, Baffin and Hudson Bays and the areas burned in West Siberia and Canada indicating trans-Arctic transport. According to the MODIS C6.1 product, there was a strong and very strong correlation between the area burned in Fenno-Scandinavia and AOD over the Kara and Laptev Seas airsheds, respectively.

The three AOD products showed positive anomalies (AOD (P1)-AOD (JJASO of the year)) in AOD. They were largest in 2019 over the entire Arctic both over ocean and land due to the severe fires in Siberia and Canada (**Figure 5(b)**, **Figure 5(d)**, **Figure 5(f)** and **Figure 4(a)**). Typically, anomalies were the largest for the MODIS C6.1 product because it also provided higher AOD values than the two other products (cf. **Table 1**; **Figure 3**). According to the CALIOP product, a slightly lower positive anomaly than in 2019 occurred over the Bering Sea in 2018 due to severe fires in Siberia (**Figure 5(b)**). On the contrary, the MAIAC product provided a negative anomaly.

MODIS C6.1 and MAIAC provided higher correlations between the 15-years (2006-2020) JJASO mean AOD over the basins and the area burned in the various wildfire regions than CALIOP (**Figure 5(a)**, **Figure 5(c)** and **Figure 5(e)**). This finding can be explained by the higher temporal resolution and larger spatial coverage of the former products than the CALIOP product.

The heatmaps of JJASO anomalies in the various years compared to the P1 mean AOD suggest that the MODIS C6.1 product is more sensitive to changes in AOD than the other two products. For example, the AOD anomaly in response to

the extremely severe fire season in Siberia of 2019 is most distinctly featured by the MODIS C6.1 product (Figure 5(b), Figure 5(d) and Figure 5(f)).

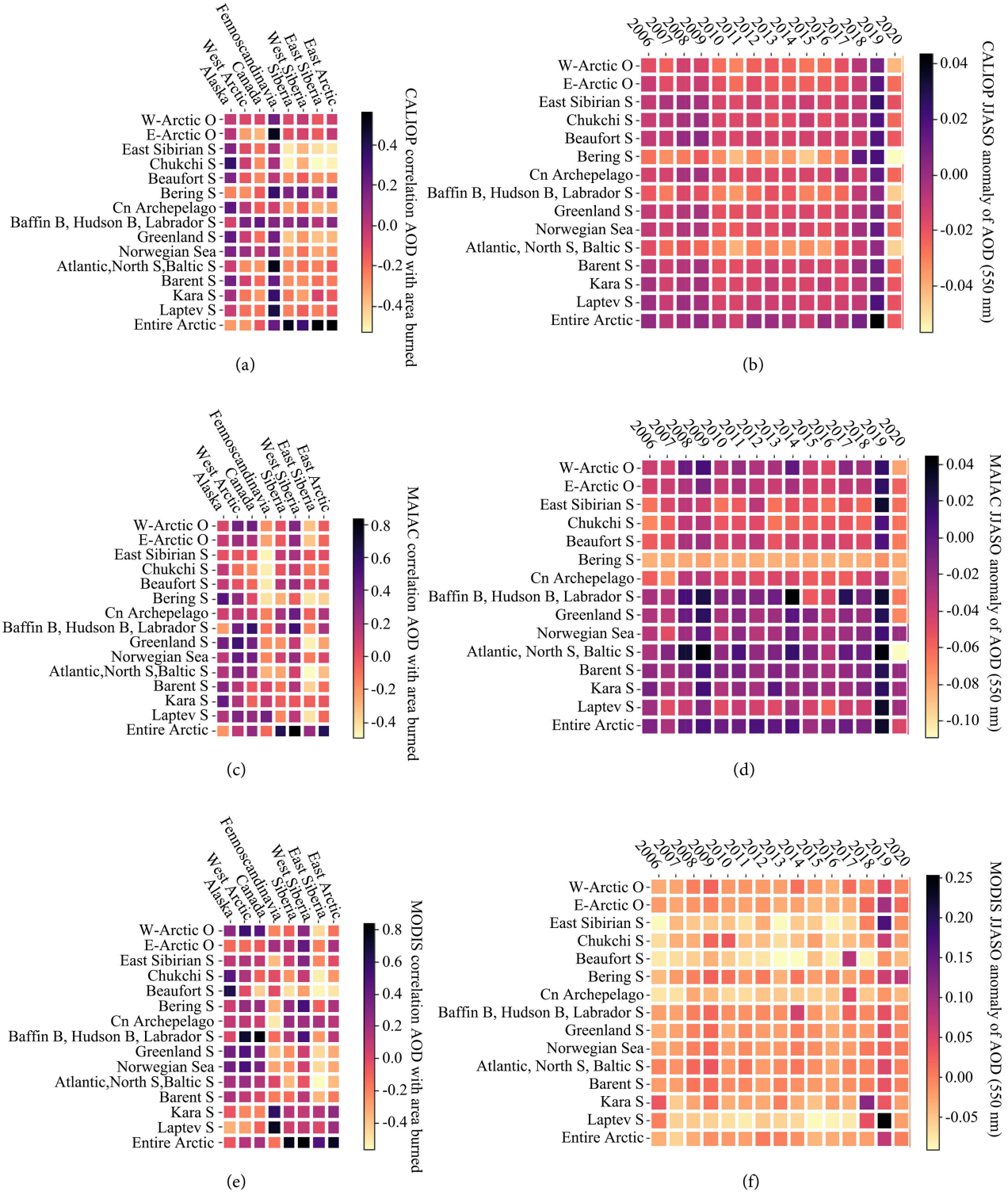

Figure 5. Heatmaps of the relation of mean JJASO 2006-2020 AOD over various airsheds with the area burned for (a) CALIOP, (c) MAIAC, and (e) MODIS C6.1; JJASO AOD anomalies (mean AOD of JJASO minus mean AOD 2006-2012) in the airsheds for (b) CALIOP, (d) MAIAC, and (f) MODIS C6.1. Legends differ among panels.

3.2. Impacts on AOD Due to Shipping

In all years, the MODIS AOD product showed increased JJASO AOD values over stretches of the Lena and Yenisei Rivers, in the Laptev Sea, in the Bering Sea and Chukchi Sea out of the Red Dog Mine Seaport (e.g. **Figure 3(e)** and **Figure 3(f)**). However, the magnitude of AOD in these areas differed over the years. Typically, AOD increased with the progression of time in the shipping season due to the sea-ice melting, and in Siberia, river break-up moving north. Interestingly, the temporal evolution of the annual minimum closely matched that of the annual mean sea-ice extent (**Figure 4(b)**).

Obviously, correlations between ship traffic on the various Arctic routes and satellite-retrieved AOD over the airsheds are very weak. However, there seems to be a weak to moderate negative correlation between ship traffic in the Eastern Arctic basins and AOD in the airsheds over the western Arctic basins, and vice versa (**Figure 6(a)**, **Figure 6(c)** and **Figure 6(e)**). All three products show, for instance, a negative moderate correlation between ship traffic on the NEP and the AOD over the Beaufort and Chukchi Seas. This correlation is expected because ships on the NEP don't cross these Seas.

Typically, MODIS C6.1 AOD shows higher positive correlations between ship traffic and AOD over the basins in which the shipping routes are located than CALIOP or MAIAC-retrieved AOD (**Figure 6(a)**, **Figure 6(c)** and **Figure 6(e)**).

In the Western Arctic airshed, AOD shows a weak positive correlation with both mean and minimum sea-ice extent for all three aerosol products (**Figure 6(b)**, **Figure 6(d)** and **Figure 6(f)**). On the contrary, according to the CALIOP and MODIS C6.1 data, AOD increases with decreasing mean sea-ice extent, in the Eastern Arctic airshed. The heatmaps suggest that as the area of (minimum) sea-ice decreases, AOD increases over the eastern Arctic. This finding can be explained by an increase in emissions due to more ship traffic in the NSR along the Siberian coast.

3.3. Changes in AOD between 2006-2012 and 2014-2020

At first glance, the P1 and P2 (not shown) mean AOD distributions showed broadly similar features as those for 2006-2020 (cf. **Figure 7**).

Differences P2 minus P1 (**Figure 8**) exceed 0.1 over Siberia for all three products. This finding is consistent with the more severe and stronger emissions from wildfires in P2 than in P1 (cf. **Figure 4(a)**). However, the spatial extent with increased AOD was largest for the MODIS C6.1 product and smallest for the CALIOP product. This result is due to the different temporal and spatial scales of the AOD products before resampling. As aforementioned, the MAIAC product provides daily mean AOD. Consequently, particles from fast-extinguished wildfires may have already settled or the concentration is diluted due to averaging [49]. Because CALIOP has low spatial resolution particles from wildfires are more likely outside the field of view, while the coarse temporal resolution may miss events of elevated AOD between overpasses. On the contrary, the MODIS 6.1 AOD

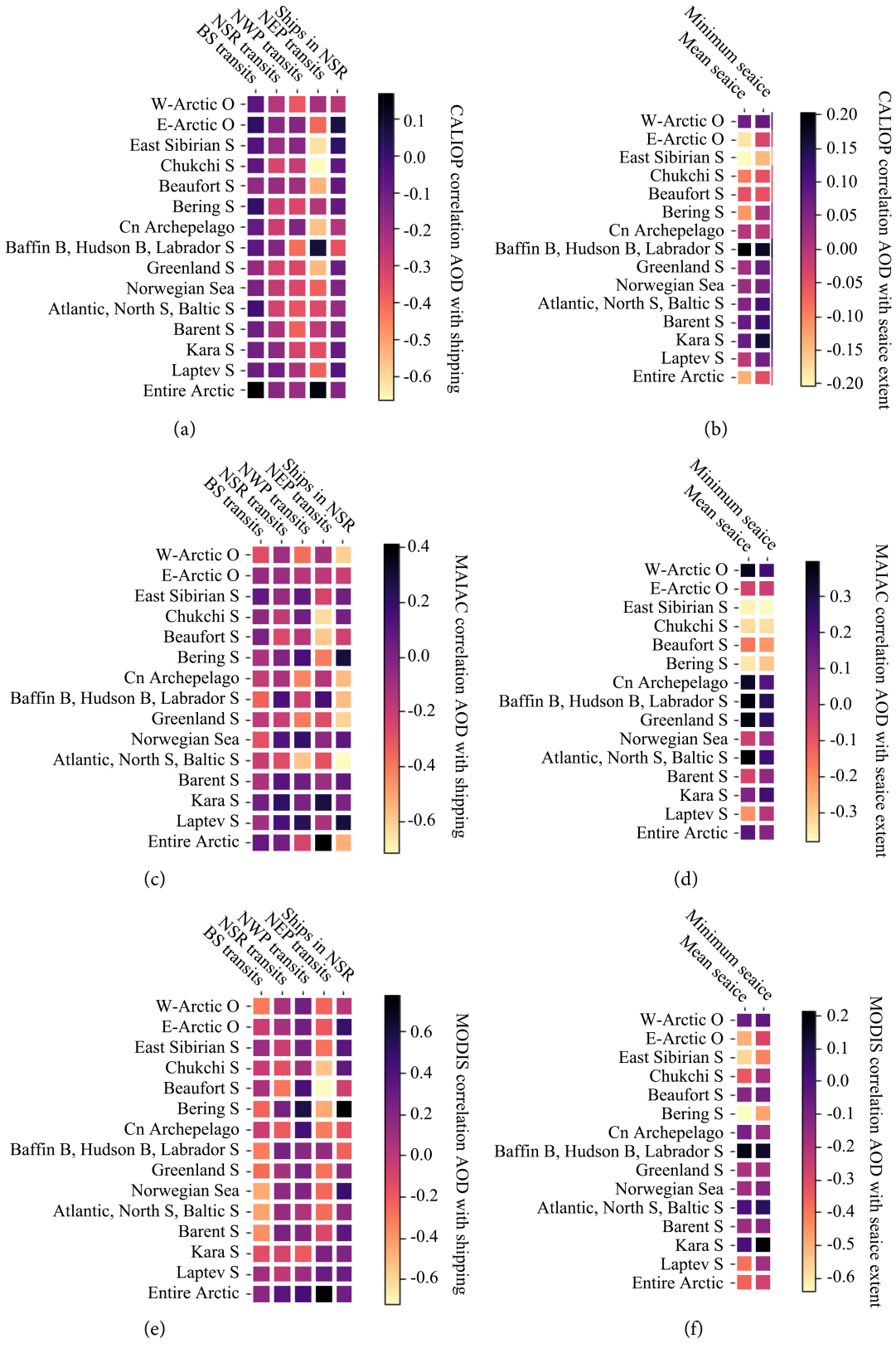

Figure 6. Heatmaps of the relation of mean JJASO 2006-2020 AOD over various airsheds with traffic on the Arctic shipping routes for (a) CALIOP, (c) MAIAC, and (e) MODIS C6.1; and mean and minimum sea-ice extent for (b) CALIOP, (d) MAIAC, and (f) MODIS C6.1. Legends differ among panels.

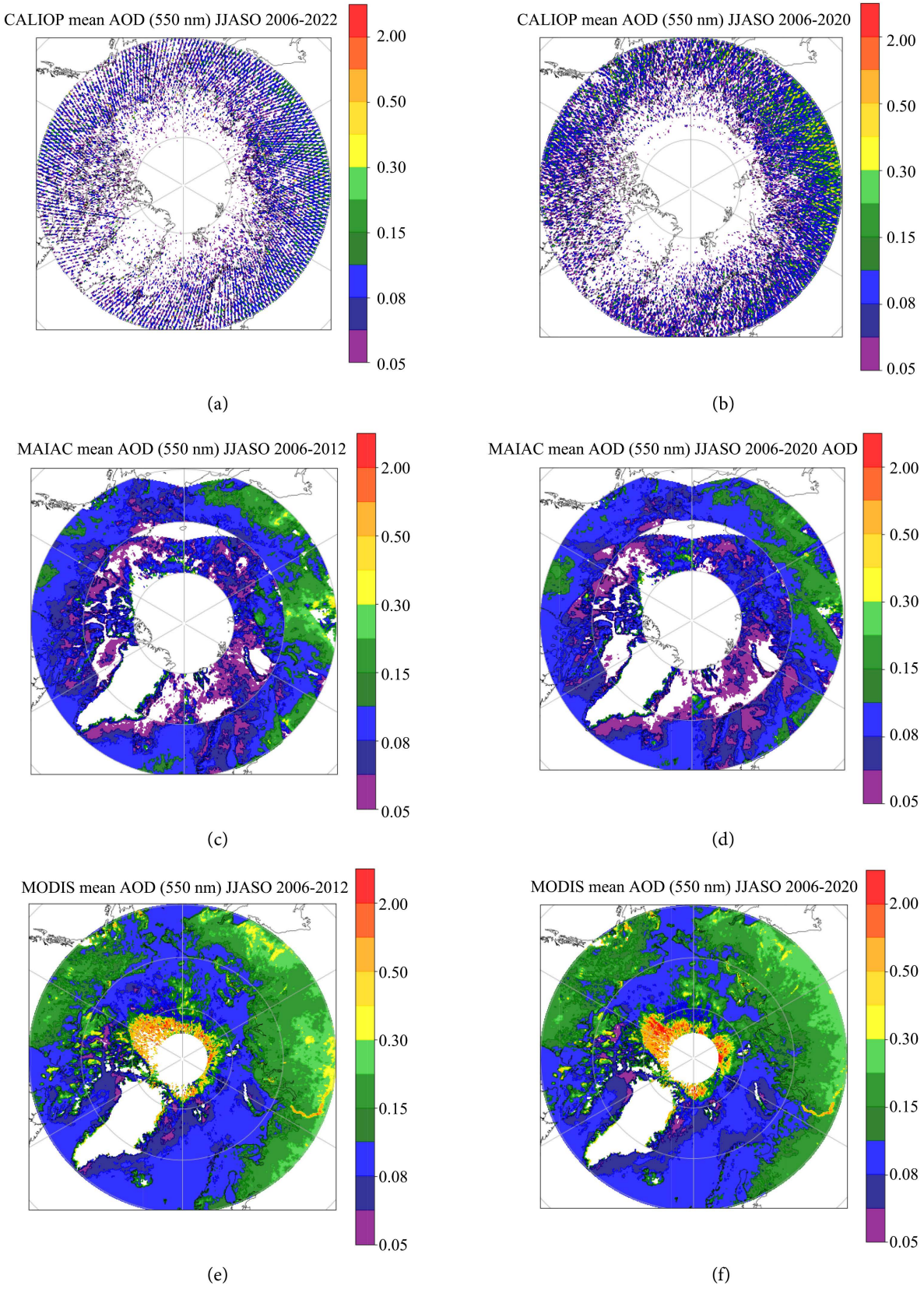

Figure 7. Mean spatial distribution of (a), (c), (e) 2006-2012 JJASO (P1) AOD, and (b), (d), (f) 2006-2020 JJASO AOD as obtained by (a), (b) CALIOP, (c), (d) MAIAC, (e), (f) MODIS C6.1. White areas indicte no retrievals.

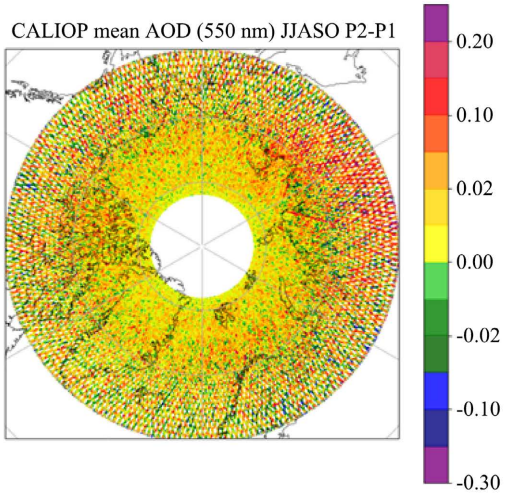

(a)

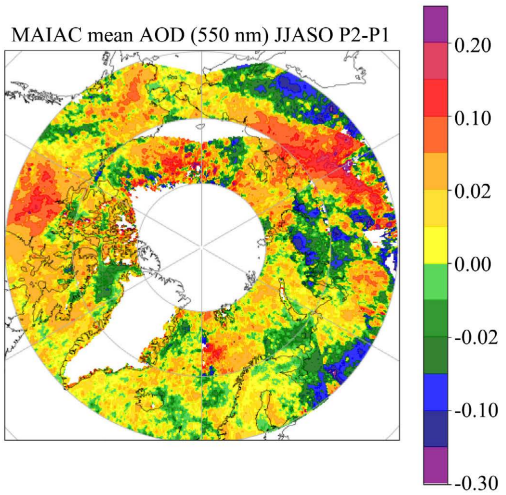

(b)

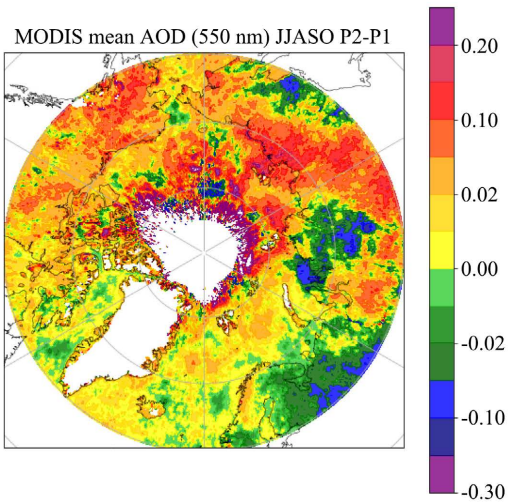

(c)

Figure 8. 2014-2020 JJASO minus 2006-2012 JJASO mean spatial distribution of AOD for (a) CALIOP, (b) MAIAC, (c) MODIS C 6.1. White areas indicate no retrievals.

values represent the AOD during the respective overpasses. Because scans have notable overlap in the high Arctic the MODIS C6.1 AOD product has the highest temporal resolution. Consequently, the likelihood to miss events of elevated AOD is the smallest. Furthermore, resampled AOD represents the mean AOD at the times of the overpasses for a respective grid cell, and not a daily mean as in the case of the MAIAC data [49].

The JJASO 2006-2020 CALIOP, MAIAC and MODIS AOD medians were below 0.0001 for all regions listed in **Table 1** except the East Arctic Ocean (0.001, 0.002, 0.038) and Arctic-wide (0.021, 0.101, 0.111).

The magnitudes of decadal changes varied among the AOD products (**Table 2**). According to the CALIOP product and MODIS C 6.1 product, AOD increased Arctic-wide, while the MAIAC product suggested a slight decrease. The AOD products indicated an increase in AOD over each ocean basin except for the CALIOP product over the Atlantic, Beaufort, North and Baltic Seas, and the MAIAC product over the Barents Sea, Atlantic, North and Baltic Seas. According to the CALIOP product, AOD experienced no change over the Beaufort Sea.

All three products captured increased AOD as expected for the known increase of ship emissions around Svalbard that occurred during P2 (**Figure 8**). However, the location of maximum increases differed among the products. These differences can be partly explained by the different spatiotemporal resolutions of the products. For more on the scaling impacts see [49].

Table 2. Change per decade in JJASO AOD, and percentage change in JJASO AOD from P1 to P2 with respect to P1 in various airsheds over the Arctic Ocean and Arctic-wide according to the AOD products.

Regions	Decadal change in JJASO AOD			Change from P1 to P2 (%)		
	CALIOP	MAIAC	MODIS C6.1	CALIOP	MAIAC	MODIS C6.1
West-Arctic Ocean	0.004	0.009	0.017	5.8	6.9	11.3
East-Arctic Ocean	0.003	0.000	0.025	5.1	0.1	14.0
East-Siberian Sea	0.004	0.016	0.063	11.0	13.5	28.5
Chukchi Sea	0.002	0.003	0.003	4.2	2.2	1.6
Beaufort Sea	<0.0001	0.005	0.034	−0.6	5.4	16.0
Bering Sea	0.018	0.010	0.025	22.0	7.9	15.1
Canadian Archipelago	0.007	0.024	0.056	14.8	20.2	33.7
Baffin & Hudson Bays, Labrador Sea	0.005	0.020	0.023	7.9	15.3	17.7
Greenland Sea	0.001	0.000	0.010	2.7	<0.01	8.1
Norwegian Sea	0.005	0.005	0.013	10.1	5.1	10.0
Atlantic, North and Baltic Seas	−0.005	−0.002	0.001	−5.7	−1.2	0.6
Barents Sea	0.003	−0.003	0.006	7.1	−2.5	4.4
Kara Sea	0.001	0.005	0.025	2.1	5.6	14.0
Laptev Sea	0.001	0.013	0.067	2.8	10.3	30.3
Entire Arctic	0.007	−0.005	0.023	13.2	−4.1	11.7

In 2015, the sulfur emissions in the North and Baltic Seas emission control area were tightened. In the airshed over the northern Baltic Sea, MODIS C6.1 and MAIAC AOD decreased in P2 as compared to P1. These decreases can be explained by tightened regulations for sulfur emissions (Figure 8(b)). For the Atlantic-North-and Baltic Seas airshed, MODIS C6.1 mean AOD increased in P2 as compared to P1. On the contrary, MAIAC and CALIOP AOD decreased in P2 with CALIOP showing the largest decrease (Table 2). The sign changes between MAIAC and MODIS C6.1 AOD changes can be explained by the large amounts of missing MAIAC data over the Atlantic. In the case of CALIOP AOD, the likelihood of detecting ship emissions is much lower than for the other two aerosol products. This is due to CALIOP's coarse temporal resolution and very small swath.

4. Summary and Conclusions

We resampled 2006-2020 June to October (both included) Terra-Aqua MODIS C6.1, MAIAC and CALIOP AOD-data on a 0.25˚ × 0.25˚ grid for each day to examine whether AOD has changed over the Arctic north of 59.75˚N due to changes in Arctic shipping. To achieve this goal we calculated AOD means, standard deviations, skewness, and kurtosis and determined the median for each shipping season (June to October) for each grid cell. Furthermore, we calculated these quantities for P1 (2006-2012) and P2 (2014-2020). These quantities were analyzed for hotspots of ship traffic identified by high standard deviation, skewness to the right, and the difference between the median and mean at the grid-cell level. Heatmaps of the correlation between AOD and ship traffic as well as AOD and fire emissions for the airsheds over various Arctic Ocean basins and the entire Arctic for each year's shipping season served to assess causes of AOD changes.

The medians, means and higher order moments of shipping seasons and periods indicate the aerosol products captured the observed inter-annual variability in wildfire occurrence. Furthermore, they detected the more severe wildfire emissions over Siberia during P2. However, the AOD values differed notably among products with typically CALIOP providing lower values than MAIAC. Except for the Baffin & Hudson Bays, Labrador Sea, Norwegian Sea and the Atlantic, North and Baltic Seas airsheds, MODIS C6.1 mean AOD was an order of magnitude higher than that of MAIAC (Table 1).

Because the combined Terra-Aqua MODIS datasets have the most daily data, the likelihood of detecting elevated AOD due to increased shipping was the largest in the MODIS data. Due to its higher temporal resolution, MODIS C6.1 AOD captures the ship traffic on the Siberian rivers (Figure 7(e) and Figure 7(f)). All three AOD products capture the increase of emissions from ships berthing near Svalbard that occurred in P2 as compared to P1 (Figure 8).

All three AOD products also suggest that except for the airsheds over the Atlantic-North-and-Baltic-Seas, Beaufort Sea, and Barents Sea, AOD was higher in

P2 than in P1. However, over the entire Arctic (ocean and land), MAIAC retrieved AOD was lower in P2 than in P1, while the opposite was true for the CALIOP and MODIS C6.1 retrieved AOD. This finding may be due to the MAIAC AOD product's design for overland detection.

Our study suggests that the MAIAC retrievals may miss short trans-Arctic AOD events, such as the transport of aerosols from fast-extinguished fires or emissions from traveling ships. The reasons are the retrievals' restrictions on glint and elevation (leading to missing data) and the fact that MAIAC provides daily AOD means. Furthermore, the study suggests that the temporal resolution of about 16 days and the low spatial coverage (just 5 km along the nadir line) of the CALIOP AOD product are too coarse to capture changes in AOD due to traveling ships on a shipping-season basis.

Based on the results of this and previous studies on the accuracy of AOD retrieved over the Arctic (e.g., [49]), MODIS C6.1 might be the most suitable for the detection of long-term changes in AOD caused by increased ship traffic in the Arctic. However, this detection of AOD changes might be qualitative. Therefore, it is better quantified as a fraction of the AOD of a reference period.

Acknowledgements

We thank the MODIS, MAIAC, and CALIOP PIs, Co-Is, and staff for establishing and maintaining the data, and algorithms used in this investigation. We appreciate the assistance of Tyler Summers in downloading the MODIS data, and the anonymous reviewers' fruitful comments and helpful discussion. This research was funded by NASA grant 80NSSC19K0981. Mariel Friberg's research was supported by an appointment to the NASA Postdoctoral Program at the NASA Goddard Space Flight Center, administered by Universities Space Research Association under contract with NASA.

Conflicts of Interest

The authors declare no conflicts of interest regarding the publication of this paper.

References

[1] Law, K.S. and Stohl, A. (2007) Arctic Air Pollution: Origins and Impacts. *Science*, **315**, 1537-1540. https://doi.org/10.1126/science.1137695

[2] Law, K.S., Stohl, A., Quinn, P.K., Brock, C.A., Burkhart, J.F., Paris, J.-D., Ancellet, G., Singh, H.B., Roiger, A., Schlager, H., Dibb, J.E., Jacob, D.J., Arnold, S.R., Pelon, J. and Thomas, J.L. (2014) Arctic Air Pollution: New Insights from POLARCAT-IPY. *Bulletin of the American Meteorological Society*, **95**, 1873-1895. https://doi.org/10.1175/BAMS-D-13-00017.1

[3] Corbett, J.J., Lack, D.A., Winebrake, J.J., Harder, S., Silberman, A.J. and Gold, M. (2010) Arctic Shipping Emissions Inventories and Future Scenarios. *Atmospheric Chemistry and Physics*, **10**, 9689-9704. https://doi.org/10.5194/acp-10-9689-2010

[4] Jacob, D.J., Crawford, J.H., Maring, H., Clarke, A.D., Dibb, J.E., Emmons, L.K.,

Ferrare, R.A., Hostetler, C.A., Russell, P.B., Singh, H.B., Thompson, A.M., Shaw, G.E., McCauley, E., Pederson, J.R. and Fisher, J.A. (2010) The Arctic Research of the Composition of the Troposphere from Aircraft and Satellites (ARCTAS) Mission: Design, Execution, and First Results. *Atmospheric Chemistry and Physics*, **10**, 5191-5212. https://doi.org/10.5194/acp-10-5191-2010

[5] Marelle, L., Thomas, J.L., Raut, J.-C., Law, K.S., Jalkanen, J.-P., Johansson, L., Roiger, A., Schlager, H., Kim, J., Reiter, A. and Weinzierl, B. (2015) Air Quality and Radiative Impacts of Arctic Shipping Emissions in the Summertime in Northern Norway: From the Local to the Regional Scale. *Atmospheric Chemistry and Physics Discussion*, **15**, 18407-18457. https://doi.org/10.5194/acpd-15-18407-2015

[6] Seinfeld, J.H. and Pandis, S.N. (1997) Atmospheric Chemistry and Physics: From Air Pollution to Climate Change. Wiley, Hoboken.

[7] Huang, K. and Fu, J.S. (2016) A Global Gas Flaring Black Carbon Emission Rate Dataset from 1994 to 2012. *Scientific Data*, **3**, Article No. 160104. https://doi.org/10.1038/sdata.2016.104

[8] Anejionu, O.C.D., Blackburn, G.A. and Whyatt, J.D. (2015) Detecting Gas Flares and Estimating Flaring Volumes at Individual Flow Stations Using MODIS Data, *Remote Sensing of Environment*, **158**, 81-94. https://doi.org/10.1016/j.rse.2014.11.018

[9] Roiger, A., Thomas, J.L., Schlager, H., Law, K.S., Kim, J., Schäfler, A., Weinzierl, B., Dahlkötter, F., Krisch, I., Marelle, L., Minikin, A., Raut, J.C., Reiter, A., Rose, M., Scheibe, M., Stock, P., Baumann, R., Bouarar, I., Clerbaux, C., George, M., Onishi, T. and Flemming, J. (2014) Quantifying Emerging Local Anthropogenic Emissions in the Arctic Region: The Access Aircraft Campaign Experiment. *Bulletin of the American Meteorological Society*, **96**, 441-460. https://doi.org/10.1175/BAMS-D-13-00169.1

[10] Bai, J. (2015) The Imo Polar Code: The Emerging Rules of Arctic Shipping Governance. *The International Journal of Marine and Coastal Law*, **30**, 674-699. https://doi.org/10.1163/15718085-12341376

[11] USCG (2015) Report of the Investigation into the Circumstances Surrounding the Multiple Related Casualties and Grounding of the Modu Kulluk on December 31, 2012. https://usa.oceana.org/report-investigation-circumstances-surrounding-multiple-related-marine-casualties-and-grounding-modu/

[12] Federal State Budgetary Institution, N.S.R.A. (2022) List of Applications. http://www.nsra.ru/ru/rassmotrenie_zayavleniy/perechen_zayavlenii.html

[13] National Ocean Economics Program (2017) Arctic Ocean Transportation Shipping Data by Sector. https://oceaneconomics.org/arctic/arctic_transport/ship_search.aspx

[14] National Ocean Economics Program (2016) Arctic Fisheries. https://oceaneconomics.org/arctic/fisheries/

[15] Marine Traffic (2023) MarineTraffic: Global Ship Tracking Intelligence. https://www.marinetraffic.com/en/ais/home/

[16] Stroeve, J., Serreze, M., Holland, M., Kay, J., Malanik, J. and Barrett, A. (2012) The Arctic's Rapidly Shrinking Sea Ice Cover: A Research Synthesis. *Climatic Change*, **110**, 1005-1027. https://doi.org/10.1007/s10584-011-0101-1

[17] Pizzolato, L., Howell, S.L., Derksen, C., Dawson, J. and Copland, L. (2014) Changing Sea Ice Conditions and Marine Transportation Activity in Canadian Arctic Waters between 1990 and 2012. *Climatic Change*, **123**, 161-173.

https://doi.org/10.1007/s10584-013-1038-3

[18] Onarheim, I.H., Eldevik, T., Smedsrud, L.H. and Stroeve, J.C. (2018) Seasonal and Regional Manifestation of Arctic Sea Ice Loss. *Journal of Climate*, **31**, 4917-4932. https://doi.org/10.1175/JCLI-D-17-0427.1

[19] Snyder, J.M. (2007) The Polar Tourism Markets. In: Snyder, J.M. and Stonehouse, B., Eds., *Prospects for Polar Tourism*, CABI, Wallingford, 51-70. https://doi.org/10.1079/9781845932473.0051

[20] Stewart, E.J., Dawson, J., Howell, S.E.L., Johnston, M.E., Pearce, T. and Lemelin, H. (2013) Local-Level Responses to Sea Ice Change and Cruise Tourism in Arctic Canada's Northwest Passage. *Polar Geography*, **36**, 142-162. https://doi.org/10.1080/1088937X.2012.705352

[21] Frey, K.E., Moore, G.W.K., Cooper, L.W. and Grebmeier, J.M. (2015) Divergent Patterns of Recent Sea Ice Cover across the Bering, Chukchi, and Beaufort Seas of the Pacific Arctic Region. *Progress in Oceanography*, **136**, 32-49. https://doi.org/10.1016/j.pocean.2015.05.009

[22] Berkman, P.A., Vylegzhanin, A.N. and Young, O.R. (2016) Governing the Bering Strait Region: Current Status, Emerging Issues and Future Options. *Ocean Development & International Law*, **47**, 186-217. https://doi.org/10.1080/00908320.2016.1159091

[23] Walsh, J.E., Fetterer, F., Scott Stewart, J. and Chapman, W.L. (2017) A Database for Depicting Arctic Sea Ice Variations Back to 1850. *Geographical Review*, **107**, 89-107. https://doi.org/10.1111/j.1931-0846.2016.12195.x

[24] Huntington, H.P., Daniel, R., Hartsig, A., Harun, K., Heiman, M., Meehan, R., Noongwook, G., Pearson, L., Prior-Parks, M., Robards, M. and Stetson, G. (2015) Vessels, Risks, and Rules: Planning for Safe Shipping in Bering Strait. *Marine Policy*, **51**, 119-127. https://doi.org/10.1016/j.marpol.2014.07.027

[25] Eckhardt, S., Hermansen, O., Grythe, H., Fiebig, M., Stebel, K., Cassiani, M., Baecklund, A. and Stohl, A. (2013) The Influence of Cruise Ship Emissions on Air Pollution in Svalbard—A Harbinger of a More Polluted Arctic? *Atmospheric Chemistry and Physics*, **13**, 8401-8409. https://doi.org/10.5194/acp-13-8401-2013

[26] Zhan, L., Wu, M., Chen, L., Zhang, J., Li, Y. and Liu, J. (2017) The Air-Sea Nitrous Oxide Flux Along Cruise Tracks to the Arctic Ocean and Southern Ocean. *Atmosphere*, **8**, Article No. 216. http://www.mdpi.com/2073-4433/8/11/216 https://doi.org/10.3390/atmos8110216

[27] Mölders, N., Gende, S. and Pirhalla, M.A. (2013) Assessment of Cruise-Ship Activity Influences on Emissions, Air Quality, and Visibility in Glacier Bay National Park. *Atmospheric Pollution Research*, **4**, 435-445. https://doi.org/10.5094/APR.2013.050

[28] Mölders, N. and Gende, S. (2015) Impacts of Cruise-Ship Entry Quota on Visibility and Air Quality in Glacier Bay. *Journal of Environmental Protection*, **6**, 1236-1356. https://doi.org/10.4236/jep.2015.611109

[29] Mölders, N., Porter, S.E., Cahill, C.F. and Grell, G.A. (2010) Influence of Ship Emissions on Air Quality and Input of Contaminants in Southern Alaska National Parks and Wilderness Areas during the 2006 Tourist Season. *Atmospheric Environment*, **44**, 1400-1413. https://doi.org/10.1016/j.atmosenv.2010.02.003

[30] Corbett, J.J., Wang, H. and Winebrake, J.J. (2009) The Effectiveness and Costs of Speed Reductions on Emissions from International Shipping. *Transportation Research Part D: Transport and Environment*, **14**, 593-598. https://doi.org/10.1016/j.trd.2009.08.005

[31] Ramanathan, V., Crutzen, P.J., Kiehl, J.T. and Rosenfeld, D. (2001) Aerosols, Cli-

mate, and the Hydrological Cycle. *Science*, **294**, 2119-2124. https://doi.org/10.1126/science.1064034

[32] Zhang, Y., Wen, X.-Y. and Jang, C.J. (2010) Simulating Chemistry-Aerosol-Cloud-Radiation-Climate Feedbacks over the Continental U.S. Using the Online-Coupled Weather Research Forecasting Model with Chemistry (WRF/Chem). *Atmospheric Environment*, **44**, 3568-3582. https://doi.org/10.1016/j.atmosenv.2010.05.056

[33] Zhao, C. and Garrett, T.J. (2015) Effects of Arctic Haze on Surface Cloud Radiative Forcing. *Geophysical Research Letters*, **42**, 557-564. https://doi.org/10.1002/2014GL062015

[34] Mölders, N. (2011) Land-Use and Land-Cover Changes: Impact on Climate and Air Quality. Springer, New York, **44**, 193. https://doi.org/10.1007/978-94-007-1527-1

[35] Quinn, P.K., Shaw, G., Andrews, E., Dutton, E.G., Ruoho-Airola, T. and Gong, S.L. (2007) Arctic Haze: Current Trends and Knowledge Gaps. *Tellus B*: *Chemical and Physical Meteorology*, **59**, 99-114. https://doi.org/10.1111/j.1600-0889.2006.00236.x

[36] Pirhalla, M.A., Gende, S. and Mölders, N. (2014) Fate of Particulate Matter from Cruise-Ship Emissions in Glacier Bay during the 2008 Tourist Season. *Journal of Environmental Protection*, **4**, 1235-1254. https://doi.org/10.4236/jep.2014.512118

[37] Mölders, N. and Kramm, G. (2018) Climatology of Air Quality in Arctic Cities—Inventory and Assessment. *Open Journal of Air Pollution*, **7**, 48-93. https://doi.org/10.4236/ojap.2018.71004

[38] Holben, B.N., Eck, T.F., Slutsker, I., Tanré, D., Buis, J.P., Setzer, A., Vermote, E., Reagan, J.A., Kaufman, Y.J., Nakajima, T., Lavenu, F., Jankowiak, I. and Smirnov, A. (1998) AERONET—A Federated Instrument Network and Data Archive for Aerosol Characterization. *Remote Sensing of Environment*, **66**, 1-16. https://doi.org/10.1016/S0034-4257(98)00031-5

[39] Smirnov, A., Holben, B.N., Slutsker, I., Giles, D.M., McClain, C.R., Eck, T.F., Sakerin, S.M., Macke, A., Croot, P., Zibordi, G., Quinn, P.K., Sciare, J., Kinne, S., Harvey, M., Smyth, T.J., Piketh, S., Zielinski, T., Proshutinsky, A., Goes, J.I., Nelson, N.B., Larouche, P., Radionov, V.F., Goloub, P., Krishna Moorthy, K., Matarrese, R., Robertson, E.J. and Jourdin, F. (2009) Maritime Aerosol Network as a Component of Aerosol Robotic Network. *Journal of Geophysical Research*: *Atmospheres*, **114**. https://doi.org/10.1029/2008JD011257

[40] CMTS (2015) A 10-Year Projection of Maritime Activity in the U.S. Arctic Region. 73. https://pame.is/document-library/shipping-documents/arctic-ship-traffic-data-documents/reports/451-a-10-year-projection-of-maritime-activity-in-the-u-s-arctic-region/file

[41] Winker, D.M., Hunt, W.H. and McGill, M.J. (2007) Initial Performance Assessment of CALIOP. *Geophysical Research Letter*, **34**. https://doi.org/10.1029/2007GL030135

[42] Vaughan, M.A., Young, S.A., Winker, D.M., Powell, K.A., Omar, A.H., Liu, Z.Y., Hu, Y.X. and Hostetler, C.A. (2004) Fully Automated Analysis of Space-Based Lidar Data: An Overview of the CALIPSO Retrieval Algorithms and Data Products. In: Singh, U.N., Ed., *Laser Radar Techniques for Atmospheric Sensing*, *SPIE Proceedings*, Vol. 5575, SPIE, Bellingham, 16-30. https://doi.org/10.1117/12.572024

[43] NASA (2018) CALIPSO Data User's Guide. https://www-calipso.larc.nasa.gov/resources/calipso_users_guide/

[44] Roy, D.P., Borak, J.S., Devadiga, S., Wolfe, R.E., Zheng, M. and Descloitres, J. (2002) The MODIS Land Product Quality Assessment Approach. *Remote Sensing of Envi-*

ronment, **83**, 62-76. https://doi.org/10.1016/S0034-4257(02)00087-1

[45] Lyapustin, A., Wang, Y., Korkin, S. and Huang, D. (2018) MODIS Collection 6 MAIAC Algorithm. *Atmospheric Measurement Techniques*, **11**, 5741-5765. https://doi.org/10.5194/amt-11-5741-2018

[46] NASA (2019) MODIS MAIAC Data Collection. https://lpdaac.usgs.gov/products/mcd19a2v006

[47] Remer, L.A., Mattoo, S., Levy, R.C. and Munchak, L.A. (2013) MODIS 3 km Aerosol Product: Algorithm and Global Perspective. *Atmospheric Measurement Techniques*, **6**, 1829-1844. https://doi.org/10.5194/amt-6-1829-2013

[48] Winker, D.M., Vaughan, M.A., Omar, A., Hu, Y., Powell, K.A., Liu, Z., Hunt, W.H. and Young, S.A. (2009) Overview of the CALIPSO Mission and CALIOP Data Processing Algorithms. *Journal of Atmospheric and Oceanic Technology*, **26**, 2310-2323. https://doi.org/10.1175/2009JTECHA1281.1

[49] Mölders, N. and Friberg, M. (2023) June to October Aerosol Optical Depth over the Arctic at Various Spatial and Temporal Scales in MODIS, MAIAC, CALIOP and GOES Data. *Open Journal of Air Pollution*, **12**, 1-29. https://doi.org/10.4236/ojap.2023.121001

[50] NSIDC: National Snow and Ice Data Center (2010) Multisensor Analyzed Sea Ice Extent—Northern Hemisphere (MASIE-NH), Version 1, National Snow and Ice Data Center, Boulder, Colorado.

[51] Randerson, J.T., van der Werf, G.R., Giglio, L., Collatz, G.J. and Kasibhatla, P.S. (2018) Global Fire Emissions Database, Version 4.1 (GFEDv4), Oak Ridge National Lab, Oak Ridge.

[52] Mölders, N. and Friberg, M. (2020) Using MAN and Coastal AERONET Measurements to Assess the Suitability of MODIS C6.1 Aerosol Optical Depth for Monitoring Changes from Increased Arctic Shipping. *Open Journal of Air Pollution*, **9**, 77-104. https://doi.org/10.4236/ojap.2020.94006

[53] Mölders, N. and Edwin, S.G. (2018) Review of Black Carbon in the Arctic: Origin, Measurement Methods, and Observations. *Open Journal of Air Pollution*, **7**, 181-213. https://doi.org/10.4236/ojap.2018.72010